

# Static and dynamic anomalies in a repulsive spherical ramp liquid: Theory and simulation

Pradeep Kumar,<sup>1</sup> Sergey V. Buldyrev,<sup>2,1</sup> Francesco Sciortino,<sup>3</sup> Emanuela Zaccarelli,<sup>3</sup> and H. Eugene Stanley<sup>1</sup>

<sup>1</sup>*Center for Polymer Studies and Department of Physics, Boston University, Boston, Massachusetts 02215, USA*

<sup>2</sup>*Department of Physics, Yeshiva University, 500 W. 185th Street, New York, New York 10033, USA*

<sup>3</sup>*Dipartimento di Fisica and INFM CRS-SOFT, Complex Dynamics in Structured Systems, Università di Roma La Sapienza, Piazzale Aldo Moro 5, I00185 Rome, Italy*

(Received 4 November 2004; published 1 August 2005)

We compare theoretical and simulation results for static and dynamic properties for a model of particles interacting via a spherically symmetric repulsive ramp potential. The model displays anomalies similar to those found in liquid water, namely, expansion upon cooling and an increase of diffusivity upon compression. In particular, we calculate the state points  $P(\rho, T)$  from the simulation and successfully compare it with the state points  $P(\rho, T)$  obtained using the Rogers-Young (RY) closure for the Ornstein-Zernike (OZ) equation. Both the theoretical and the numerical calculations confirm the presence of a line of isobaric density maxima, and lines of compressibility minima and maxima. Indirect evidence of a liquid-liquid critical point is found. Dynamic properties also show anomalies. Along constant temperature paths, as the density increases, the dynamics alternate between slowing down and speeding up, and we associate this behavior with the progressive structuring and destructuring of the liquid. Finally we confirm that mode coupling theory successfully predicts the nonmonotonic behavior of dynamics and the presence of multiple glass phases, providing strong evidence that structure (the only input of mode coupling theory) controls dynamics.

DOI: [10.1103/PhysRevE.72.021501](https://doi.org/10.1103/PhysRevE.72.021501)

PACS number(s): 64.70.Pf, 82.70.Dd, 83.10.Rs, 61.20.Ja

## I. INTRODUCTION

Water and some other liquids exhibit anomalous behavior close to their freezing lines [1,2]. Their phase diagrams have regions characterized by a negative thermal expansion coefficient, i.e., these liquids expand upon cooling at certain temperatures and pressures. Besides the density anomaly, such liquids also have other peculiar thermodynamic and dynamic behaviors [3]. For example, the isothermal compressibility increases upon cooling and the diffusivity increases upon pressurizing. Usually, the region of the diffusion anomaly is wider than the region of the density anomaly, so that the latter is completely contained in the former [4]. The anomalous behavior of the thermodynamic properties of water has been connected to the existence of a hypothetical liquid-liquid critical point in deeply supercooled states [5–8]. In the case of water, this critical point is located in an experimentally inaccessible region. Recently, using the potential energy landscape formalism, it has been argued [8] that under certain assumptions on the statistical properties of the potential energy landscape, the existence of a density anomaly must lead to the existence of a liquid-liquid critical point.

In the case of water, anomalies are thought to be related to the tetrahedrality of the interparticle potential. On average, each water molecule has four nearest neighbors connected by hydrogen bonds. However, tetrahedrality is not a necessary condition for anomalous behavior and several spherically symmetric potentials that are able to generate density and/or diffusion anomalies have been proposed [9–16]. Interestingly, such potentials may be purely repulsive, providing evidence that different microscopic mechanisms can generate density anomalies. These potentials can be regarded as the simplest models which yield water-type thermodynamic and dynamic anomalies and it is important to fully characterize their thermodynamic and dynamic behavior. An additional

advantage in studying spherical potentials is that their behavior can also be studied within a theoretical framework, for their thermodynamic properties can be calculated using accurate integral equation closures.

Here we study, using extensive molecular dynamics (MD) simulations, a specific, spherically symmetric repulsive potential introduced by Jagla [11–15,17] with the aim of fully characterizing both static and dynamic extreme loci in the temperature-density plane. We complement the MD study with integral theory calculations based on the (thermodynamically consistent) Rogers-Young (RY) closure, which is known to give accurate results for other repulsive potentials, such as the square shoulder potential [18] and the star polymer potential [19–21]. We also compare numerical results in the low  $T$  region with predictions based on the ideal mode-coupling theory (MCT) [22,23], which we solve using the RY static structure factors as input. We find that MCT is able to predict the nonmonotonic behavior of dynamics and the presence of multiple glass phases, providing further evidence that structure (the only input of MCT) controls dynamics in this system.

## II. METHODS

### A. Discrete molecular dynamics simulations

We study the linear ramp potential introduced by Jagla [11–15] (see Fig. 1)

$$U(r) = \begin{cases} \infty, & r < \sigma_0, \\ U_0(\sigma_1 - r)/(\sigma_1 - \sigma_0), & \sigma_0 < r < \sigma_1, \\ 0, & r > \sigma_1 \end{cases} \quad (1)$$

focusing on the specific choice of  $\lambda \equiv \sigma_1/\sigma_0 = 1.76$ , which has been studied previously by Jagla [11]. Using Monte

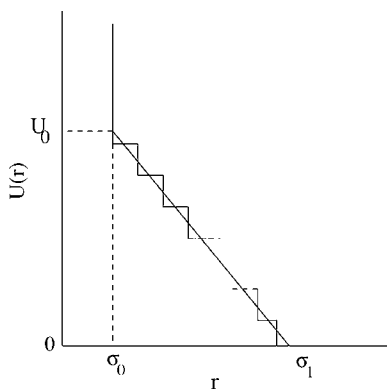


FIG. 1. Schematic representation of the repulsive ramp potential (1) and its discontinuous version (2).

Carlo simulations, Jagla showed that a density maximum is found in the liquid phase. For this choice of  $\lambda$ , the potential in Eq. (1) is a good candidate for studying the connection between thermodynamic and dynamic quantities. In order to study the dynamic properties, we apply the discrete MD method, approximating the continuous potential by a sequence of step functions with  $n$  small vertical steps,

$$U_n(r) = \begin{cases} \infty, & r < \sigma_0, \\ k\Delta U, & \sigma_1 - (k + \frac{1}{2})\Delta r < r < \sigma_1 - (k - \frac{1}{2})\Delta r, \\ 0, & r > \sigma_1 - \frac{\Delta r}{2}, \end{cases} \quad (2)$$

where  $\Delta r \equiv (\sigma_1 - \sigma_0)/(n + 1/2)$ ,  $\Delta U \equiv U_0/(n + 1/2)$ , and  $k = 1, 2, 3, \dots, n$ . The unit of length is  $\sigma_0$ , while  $U_0$  is the unit of energy. Temperature is measured in units of energy, i.e.,  $k_B = 1$ . Simulation time is measured in units of  $\sigma_0 \sqrt{m/U_0}$ , with  $m$  as the particle mass, and pressure in units of  $U_0/\sigma_0^3$ . The number density is defined as  $\rho \equiv N/L^3$ , where  $L$  is the size of the simulation box and  $N$  is the number of particles.

Standard discrete molecular dynamics (DMD) algorithm has been implemented for particles interacting with step potentials [24–26]. Between collisions, particles move along straight lines with constant velocities. When the distance between the particles becomes equal to the distance for which  $U(r)$  has a discontinuity, the velocities of the interacting particles instantaneously change (see Fig. 1.) The algorithm calculates the shortest collision time in the system and propagates the trajectories of particles from one collision to the next. Calculations of the next collision time are optimized by dividing the system into small subsystems, so that collision times are computed only between particles in neighboring subsystems. Since the total energy  $E$  is rigorously conserved, it is best to study the  $NVE$  ensemble in the cubic box of a fixed volume  $V = L^3$  with periodic boundary conditions. This method is more efficient at low densities compared to the regular molecular dynamics simulation since the velocities and positions of the atoms are updated only when they go through a collision. Another reason for choosing DMD is that it is difficult to implement continuous molecular dynamics for a hardcore potential.

We consider  $N = 1728$  particles in our simulation. For constant temperature simulations, the Berendsen thermostat is used. Berendsen thermostat with  $T_0 = 0.01$  and a small heat exchange coefficient less than  $10^{-4}$  can also be used for slowly cooling the system. During this process, the temperature of the system gradually decreases from  $T = 0.2$  to  $T = 0.01$ . The average pressure in any interval of time approximates the equilibrium pressure for the corresponding average temperature. These cooling simulations allow us to quickly obtain the entire isochore in a single run. We compared few state points obtained using standard  $NVE$  ensemble with the state points obtained using cooling and we do not find any difference between them. Analogously we can simulate the process of slow heating, which we use to estimate an upper limit of melting line.

Configurations in the  $NVE$  ensemble are saved for further processing namely at times  $t_{jk} \equiv (js^m + s^k)\Delta t$ , where  $k = 0, 1, \dots, m$  and  $j = 0, 1, \dots, j_{\max}$ . For the majority of our state points we use  $\Delta t = 0.0308$ ,  $m = 14$ ,  $j_{\max} = 100$ , and  $s = 2$ .

For each run we discard an initial equilibration period for a time larger than the correlation time at a particular state point.

The diffusion coefficient  $D$ , measured in units of  $\sigma_0 \sqrt{U_0/m}$ , is calculated as

$$D = \lim_{t \rightarrow \infty} \frac{\langle [\mathbf{r}(t') + t] - \mathbf{r}(t') \rangle_{t'}^2}{6t}, \quad (3)$$

where  $\langle \dots \rangle_{t'}$  denotes an average over all particles and over all  $t'$ . The dynamic structure factor for a given vector  $\mathbf{q}$  is defined as

$$S(\mathbf{q}, t) \equiv \left\langle \frac{1}{N} \sum_{i,j} \exp\{i\mathbf{q} \cdot [\mathbf{r}_i(t') + t] - \mathbf{r}_j(t')\} \right\rangle_{t'}, \quad (4)$$

where  $\langle \dots \rangle_{t'}$  denotes the average over all  $t'$  and  $S(\mathbf{q}) \equiv S(\mathbf{q}, 0)$  is the static structure factor. The normalized structure factor

$$\phi(\mathbf{q}, t) \equiv \frac{S(\mathbf{q}, t)}{S(\mathbf{q}, 0)} \quad (5)$$

is called the density correlator. The isotropy of the liquid allows us to average  $S(\mathbf{q}, t)$  over different  $\mathbf{q}$  with the same modulus. In the following, we bin together all  $\mathbf{q}$  within a mesh  $\Delta q = \pi/L$ .

## B. Rogers-Young closure

Integral equation theories are powerful tools for studying the structure and thermodynamic properties of liquids [27,28]. One assumes a two-body interaction potential for the particles and introduces the total pair correlation function  $h(r)$ , related to the pair distribution function  $g(r) \equiv h(r) + 1$ , and the direct correlation function  $c(r)$ . The goal is to solve the Ornstein-Zernike equation using a thermodynamically consistent closure,

$$h(r) = c(r) + \rho \int dr' c(|\mathbf{r} - \mathbf{r}'|)h(r'), \quad (6)$$

where both  $c(r)$  and  $h(r)$ —or, equivalently,  $g(r)$ —are unknown. Equation (6) in Fourier space takes the form

$$\tilde{h}(q) = \tilde{c}(q) + \rho \tilde{c}(q) \tilde{h}(q), \quad (7)$$

where  $c(q)$  is related to  $S(q)$  as  $\tilde{c}(q) = [1 - 1/S(q)]/\rho$ .

According to the particular form of the interaction potential  $U(r)$ , one can choose a certain ansatz for  $c(r)$ , which relates it to the interaction potential and to  $h(r)$  and allows one to solve Eq. (6) analytically in some cases [28] and numerically otherwise. The two frequently employed closures, Percus-Yevick (PY) or the hypernetted chain (HNC) [27], suffer from being thermodynamically inconsistent [28]. This means that although they can provide good estimates of the static structure factor, they cannot be reliably used for determining the state points  $P(\rho, T)$  of the system. More sophisticated closures have thus been developed in recent years, which have a built-in thermodynamic consistency. This is achieved by introducing an extra parameter in the ansatz, which can then be determined to fulfill such a condition.

The RY closure [29] belongs to the thermodynamically consistent group of closures obtained by appropriately mixing PY and HNC through the parameter  $\zeta$ . The ansatz for  $c(r)$  in terms of  $h(r)$  becomes

$$c(r) = \exp[-\beta U(r)] \left( 1 + \frac{\exp\{[h(r) - c(r)]z(r)\} - 1}{z(r)} - [h(r) - c(r) + 1], \right) \quad (8)$$

where  $z(r)$  is the mixing function,

$$z(r) \equiv 1 - \exp(-\zeta r). \quad (9)$$

For  $\zeta=0$ , one recovers PY closure, while for  $\zeta \rightarrow \infty$  Eq. (8) reduces to the HNC condition.

The OZ equation can be solved using Eq. (8) for a given value of  $\zeta$ . The correct solution corresponds to that value of  $\zeta$  for which the compressibilities  $K_T$ , calculated using the “virial” and the “fluctuations” routes agree, ensuring thermodynamic consistency. This allows us to reliably use the RY closure not only to calculate the static structure factor, but also the state points  $P(\rho, T)$ , as we will do in the following. Moreover, RY gives particularly good results for a purely repulsive potential, such as the studied ramp potential. It has already been successfully tested against simulations for square shoulder potentials [18], and for both experiments and simulations for the star polymer effective potential [19–21,30].

### C. Mode coupling theory

The density correlator defined in Eq. (5) is the fundamental quantity of interest in MCT, a set of generalized coupled Langevin equations which can be closed within certain approximations [22,23]. Interesting behavior of these observables arise when the dynamics of the system becomes

slower, i.e., when the dynamical behavior is of the “supercooled” type [31]. A typical two-step relaxation occurs for the density correlators on approaching dynamical arrest, indicating the emergence of two distinct time scales in the system’s structural relaxation [23,32]. A first relaxation process, the  $\beta$  relaxation, occurs at short times, and is due to particles exploring the cages formed by their nearest neighbors. A second relaxation, the  $\alpha$  relaxation, occurs at longer time scales, when particles are able to escape the cages. MCT predicts the existence of a glass transition at a characteristic temperature  $T_{\text{MCT}}$ , where the time scale of this second relaxation diverges so that the particles will always remain trapped in their cages. For  $T < T_{\text{MCT}}$  the correlators do not relax any more, reaching a finite plateau value at long  $t$ , defined as the nonergodicity parameter  $f(q) \equiv \lim_{t \rightarrow \infty} \phi(q, t)$  jumps discontinuously from zero at  $T > T_{\text{MCT}}$  to a finite (critical) value  $f_c(q)$  at  $T = T_{\text{MCT}}$ , signaling the occurrence of an ergodic (fluid) to a nonergodic (glass) transition. The transition is kinetic, i.e., nothing happens to the thermodynamic properties of the system close to  $T_{\text{MCT}}$ .

MCT predictions are often found to be in agreement with experimental [33] and simulation results [34], although in real systems the  $\alpha$ -relaxation time does not diverge, but only becomes increasingly larger. This is due to the intervention of other processes, commonly termed “hopping” processes, which restore ergodicity and are not included in the MCT treatment of the ideal glass transition described above.

In mathematical terms, the nonergodicity parameters  $f(q)$  are the long time solutions of the MCT equations, i.e.,

$$\frac{f(q)}{1 - f(q)} = m(q), \quad (10)$$

where the memory kernel  $m(q)$  is quadratic in the correlator

$$m(q) = \frac{1}{2} \int \frac{d^3k}{(2\pi)^3} \mathcal{V}(\mathbf{q}, \mathbf{k}) f(k) f(|\mathbf{q} - \mathbf{k}|), \quad (11)$$

where  $k = |\mathbf{k}|$ . The vertex functions  $\mathcal{V}$  are the coupling constants of the theory, which are given only in terms of the static structure factor and number density of the system,

$$\mathcal{V}(\mathbf{q}, \mathbf{k}) = \frac{\rho}{q^4} [\mathbf{q} \cdot (\mathbf{q} - \mathbf{k}) c(|\mathbf{q} - \mathbf{k}|) + \mathbf{q} \cdot \mathbf{k} c(k)]^2 \times S(q) S(k) S(|\mathbf{q} - \mathbf{k}|). \quad (12)$$

Equations (10) and (11) define a system of nonlinear equations with a trivial solution  $f(q) = 0$ . However, for certain values of the vertex functions, the solutions have a bifurcation point, locating the glass transition. At this transition point a solution  $f(q) > 0$  emerges. The time evolution of the density correlators is found by solving the full MCT equations,

$$\ddot{\phi}(q, t) + \Omega^2(q) \phi(q, t) + \int_0^t m(q, t - t') \dot{\phi}(q, t') dt' = 0, \quad (13)$$

where  $\Omega^2(q) \equiv q^2 / [\beta m S(q)]$  and  $m(q, t)$  is the time-dependent memory kernel

$$m(q,t) \equiv \frac{1}{2} \int \frac{d^3k}{(2\pi)^3} \mathcal{V}(\mathbf{q}, \mathbf{k}) \phi(k,t) \phi(|\mathbf{q} - \mathbf{k}|, t). \quad (14)$$

The two-step relaxation is well described by MCT through an asymptotic study of the correlators near the ideal glass solutions. The  $\alpha$  relaxation is effectively described by a stretched exponential,

$$\phi(q,t) = A_q \exp[-(t/\tau_q)^{\beta_q}], \quad (15)$$

where  $\tau_q$  is the  $q$ -dependent  $\alpha$ -relaxation time (autocorrelation time). The amplitude  $A_q$  determines the plateau value and  $\beta_q < 1$ .

MCT predicts a power-law divergence of the  $\alpha$ -relaxation time as well as a power-law decrease of the diffusivity as the system approaches the ideal glass transition. In this study, we compare the dynamic behavior evaluated from the MD simulations with corresponding MCT predictions based on the static structure factor obtained from RY closure.

### III. RESULTS

#### A. Dependence on the number of steps in the ramp

We first study how the results of molecular dynamic simulations for the potential  $U_n(r)$  in Eq. (2) converge to the results for the continuous ramp potential  $U(r)$  in (1), as  $n \rightarrow \infty$  where  $n$  is the number of approximating steps. The exact state points  $P(\rho, T)$  for systems described by a pair potential can be calculated from the partition function, i.e., by the integral  $\int \cdots \int \exp[-\sum_{i>j} U(\mathbf{r}_i - \mathbf{r}_j)/k_B T] \prod_{i=1}^N d\mathbf{r}_i$ . Replacing the continuous potential  $U(\mathbf{r}_i - \mathbf{r}_j)$  by a step function is analogous to replacing an integral by a sum in a rectangular approximation which is known to converge to the integral as  $1/n^2$ . Thus we can expect that the pressure  $P_n$  obtained in the discrete molecular dynamics for given  $n$  converges to the value for the continuous potential  $P_\infty$  as  $1/n^2$ . On the other hand, the probability for a particle to jump over a step of size  $\Delta U$  is proportional to  $\exp(-\Delta U/k_B T) = 1 - U_0/nk_B T + [U_0/k_B T + (U_0/k_B T)^2]/2n^2 - \cdots$ . The diffusion coefficient must be a differentiable function of this probability. Thus we can expect that the diffusion constant  $D_n$  in discrete MD approaches its limiting value  $D_\infty$  as  $1/n + O(1/n^2)$ . Figures 2(a) and 2(b) confirm these predictions. Particularly in Fig. 2(b), we fit  $D(n)$  with polynomials of  $1/n$  of various degrees and find that the leading term does not depend on the degree of the polynomial. In the following, we limit ourselves to the case  $n=144$  which, as shown in Figs. 2(a) and 2(b), is sufficiently close to the  $n \rightarrow \infty$  case.

#### B. Structure factors and comparison with RY

Figure 3 shows the density dependence of the structure factor, as calculated from the MD at  $T=0.063$ . At this low  $T$  the liquid, even at low densities, is significantly structured, as shown by the large amplitude of the first peak. On increasing the density, contrary to the normal liquid behavior, the amplitude of the first peak is reduced. As discussed below, the destructuring of the liquid is associated with a speed-up of the particle dynamics. If  $\rho$  is further increased, the second

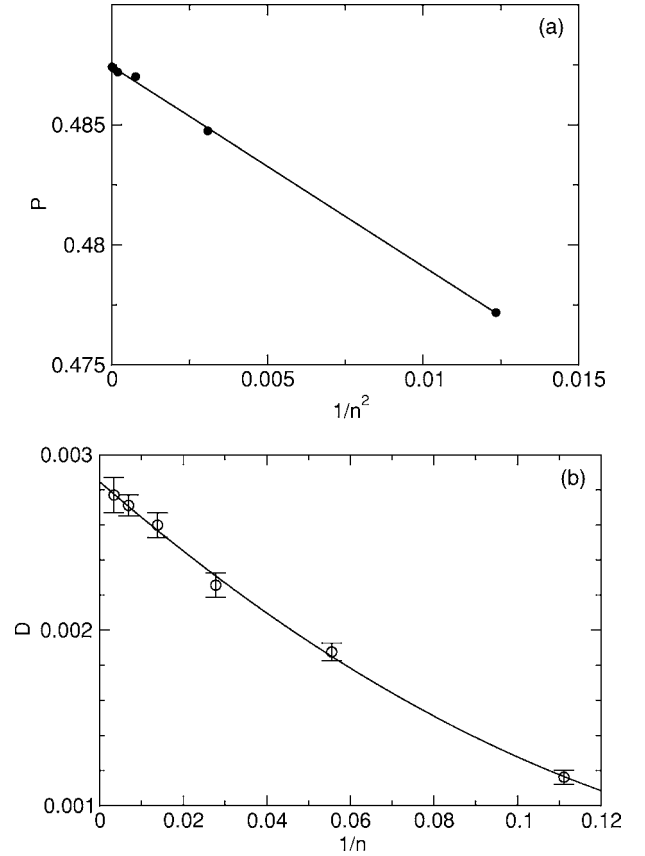


FIG. 2. (a) Pressure  $P$  as a function of  $n^{-2}$  [where  $n$  is defined in Eq. (2)] for  $T=0.063$  and  $\rho=0.260$ . (b) Diffusion coefficient  $D$  as a function of  $n^{-1}$  for the same state point. The curve is a second degree polynomial fit to the points.

peak becomes dominant and (as discussed in the following) its increase correlates with a slowing down of the dynamics. The first peak is significantly reduced and acts as a prepeak on the major peak. The crossover of the leading amplitude from the first to the second peak resembles the behavior previously discovered in star polymers of large functionality [35]. In these systems, the star-star interaction can be effec-

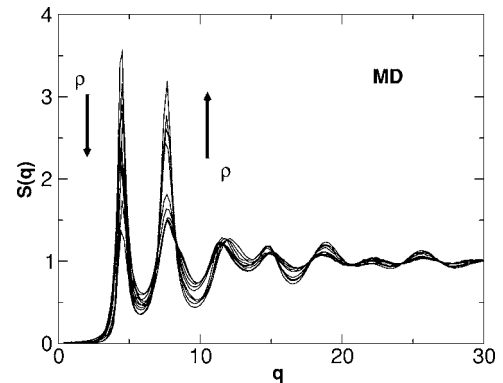


FIG. 3. Density dependence of the structure factor at  $T=0.063$ . Note the progressive reduction of the amplitude of the first peak and the progressive increase of the second peak on increasing  $\rho$ . Different curves refer to  $\rho=0.272, 0.296, 0.322, 0.352, 0.384, 0.421, 0.464, 0.512, 0.567, 0.629$ , and  $0.702$ .

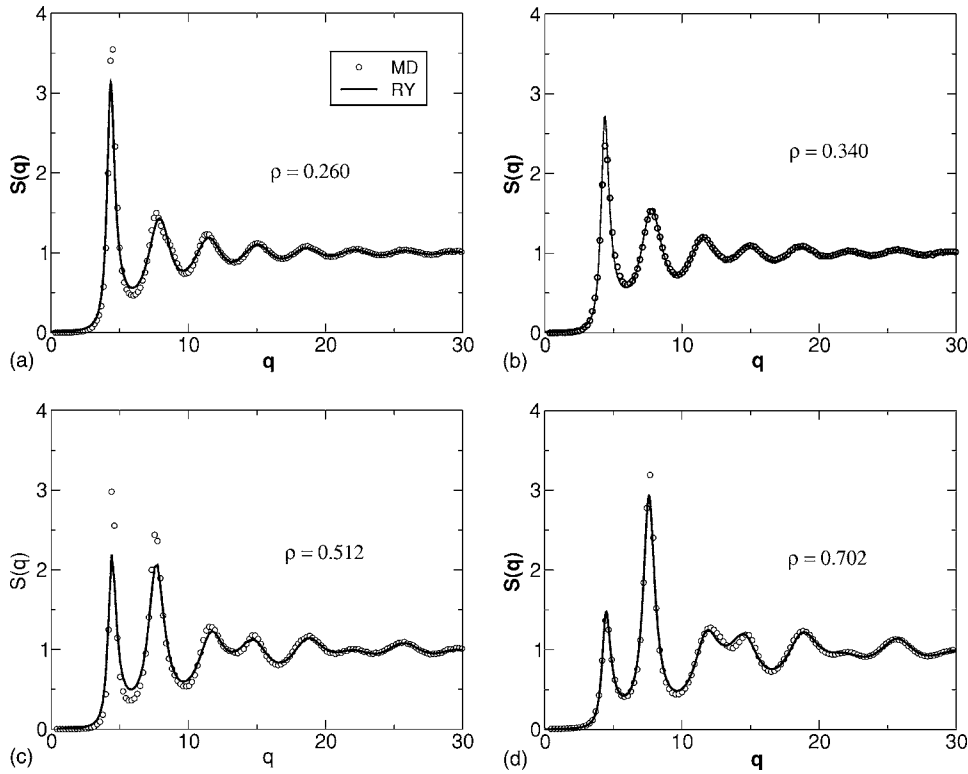


FIG. 4. Comparison of the static structure factor, obtained in simulations and in the RY closure for (a) low density  $\rho=0.260$ , (b) and (c) intermediate densities  $\rho=0.340$  and  $\rho=0.502$ , and (d) high density  $\rho=0.702$ .

tively reduced to an ultrasoft repulsive logarithmic interaction. However, the peak positions of  $S(q)$  change positions with density in this case, as opposed to what is found in the ramp potential.

Figures 4(a)–4(d) compare the static structure factor calculated using simulation data along with the results of the RY closure for several densities at  $T=0.063$ . A tolerance of  $5 \times 10^{-5}$  is used for the thermodynamic consistency. MCT with the structure factor predicted by RY integral theory provides a correct description of the  $\rho$  dependence of the dynamics. RY correctly predicts the structure factor at high densities, while for intermediate and low densities RY gives a fairly good estimate of the structure factor except that the first peak in the structure factor is lower than the one calculated from simulation. RY thus tends to underestimate the structure of the liquid.

### C. Phase diagram

Figure 5 shows the state points  $P(\rho, T)$  of the model obtained by slow cooling as discussed in Sec. II A (thin lines representing isochores) and by accurate simulations of individual state points (circles). The simulations for each density and temperature are initialized with random configurations and are equilibrated to the desired temperature using Berendsen's thermostat for a sufficient period of time. The equilibration time was estimated as the time when the density correlator  $\phi(\mathbf{q}, t)$  at the first peak of  $S(q)$  decays to zero. After equilibration, each configuration was left to run at constant energy for a time dependent on the speed of the dynamics, covering at least 10 equilibration times. The temperature of maximal density (TMD), shown by a bold line, was obtained by connecting the points on each isochore correspond-

ing to the minimal pressure, since these points correspond to the points of minimal volume due to the general relation

$$\left(\frac{\partial V}{\partial T}\right)_P = -\left(\frac{\partial P}{\partial T}\right)_V \left(\frac{\partial V}{\partial P}\right)_T \quad (16)$$

and  $(\partial V/\partial P)_T < 0$  for a mechanically stable system. Thus, volume increases upon cooling at constant pressure in the region to the left of the TMD line.

At low  $T$ , the system spontaneously crystallizes during the time of the simulation in different crystalline forms. We analyze the crystalline structures for all densities using XBS software [36]. We compare the symmetries of spontaneously grown crystalline structures with the ideal crystalline structures, proposed by Jagla (FCC, HCP, BCC, rhombohedral, simple cubic, and hexagonal) and were able to clearly identify in the majority of cases the corresponding Bravis type. Note that in our simulations we have 1728 atoms, thus we have more than 10 crystalline cells in each dimension even if the crystal has significant amount of defects. This is sufficient to check all possible symmetries by rotating structures by the specified angles and comparing projections with those of the ideal crystals. However this procedure did not allow us to clearly identify the crystalline structures in the density range between 0.26 and 0.30. In this density range, the system crystallizes with too many defects. These structures are clearly neither FCC nor rhombohedral. Consistent with Jagla's calculation [11], we find the following.

(i) At low densities  $\rho < 0.260$ , the system crystallizes into a face centered cubic crystal structure upon slow cooling (as discussed above), when the temperature reaches the values indicated by squares [36]. The crystallization is marked by a sharp drop in the potential energy, associated with a fast

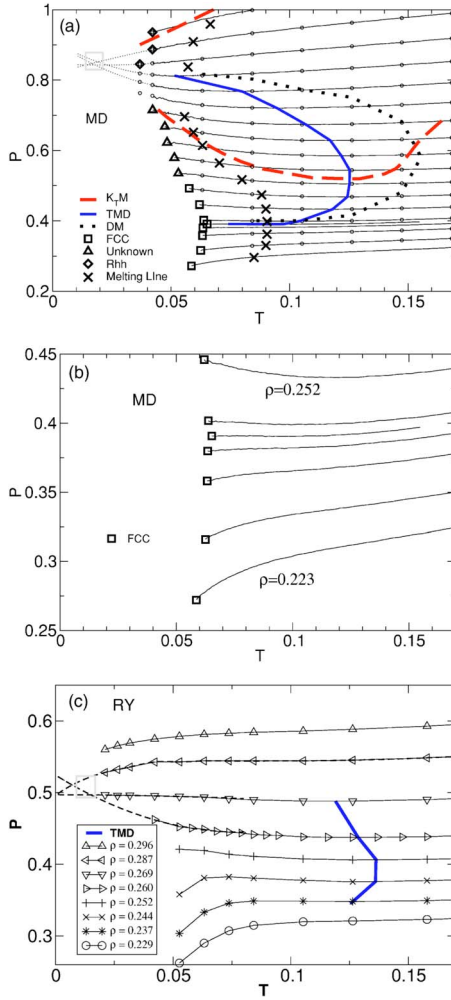


FIG. 5. (color online) (a) State points  $P(\rho, T)$  of a system of particles interacting via the potential defined in Eq. (2) with  $n = 144$ . Thin solid lines indicate  $P(T)$  for several isochores at the following values of  $\rho$ , from top to bottom: 0.378, 0.364, 0.352, 0.340, 0.328, 0.317, 0.306, 0.296, 0.287, 0.277, 0.269, 0.260, 0.252, 0.244, 0.242, 0.240, 0.237, 0.229, 0.223 obtained by slow cooling and small circles indicate state points obtained by long equilibration runs. At low  $\rho$ , lines terminate when the system crystallizes or does not equilibrate within the available simulation time. Square, triangle, and diamond symbols correspond to the temperature of spontaneous crystallization for FCC, unknown (see text) and rhombohedral crystals, respectively, while the cross symbols mark the melting of these crystals in the process of slow heating. This approximate melting line and the homogeneous nucleation line bound the region of equilibrium melting line. Note that different crystals FCC, unknown, and rhombohedral, are found for  $\rho < 0.260$ ,  $0.26 \leq \rho < 0.317$ , and  $\rho > 0.352$ , respectively. The extrapolated isochores at large  $\rho$  cross at a finite  $T$  (open box), consistent with the possibility of a liquid-liquid critical point in the region of low temperatures which cannot be investigated numerically. Also shown are the locus of density maxima  $(\partial V / \partial T)_P = 0$  (bold blue line), the locus of compressibility maxima and minima  $d[V^{-1}(\partial V / \partial P)_T] / \partial T|_P = 0$  (dashed red line), and the locus  $\partial D / \partial P|_T = 0$  (bold dotted line). (b) State points  $P(\rho, T)$  corresponding to the low densities from 0.223 to 0.252. (c) Corresponding state points  $P(\rho, T)$  obtained within the RY closure. An extrapolation of the isochores also shows the possibility of a very low temperature liquid-liquid phase transition.

release of latent heat. The line connecting these points can be regarded as a line of homogeneous nucleation. It has a marked negative slope, corresponding to the smaller density of the crystalline phase compared to liquid. An approximate estimation of melting line, which also has negative slope, is located at much higher temperatures, so that a large portion of the density anomaly region lies in the supercooled state. This situation is completely analogous to the situation in water, in which the region of the density anomaly is located near the negatively sloped freezing line. In the ramp model, the anomaly does not exist below  $\rho = 0.2432$ , where the line of the *minimal* density merges with the line of the *maximal* density. Interestingly, the slope of the homogeneous nucleation line becomes positive below this density, as in a normal liquid where the crystal phase has a larger density than in the liquid phase. This behavior may exist in stretched water at negative pressures but has never been observed experimentally or in simulations.

(ii) In the region of intermediate densities  $0.317 < \rho < 0.352$  the liquid does not crystallize and enters the glassy state below  $T < 0.037$ . We are not able to equilibrate the system below this temperature.

(iii) For  $\rho > 0.352$ , the system crystallizes into a rhombohedral crystal after being equilibrated for a long time at  $T = 0.041$ . Interestingly, the density anomaly vanishes at densities slightly lower than the density at which this crystal phase emerges. This crystalline phase is characterized by parallel columns formed by equidistantly spaced atoms. The spacing among these atoms is slightly larger than the hard core distance. Thus in this crystalline phase each atom has two neighbors in its repulsive ramp. The projection of these columns onto a perpendicular plane forms a triangular lattice with spacing approximately equal to the diameter of the repulsive ramp. The columns are shifted with respect to each other by one third of the nearest-neighbor spacing so that the atoms form three crystalline planes, perpendicular to the columns. In each of these planes atoms form a triangular lattice with a spacing  $\sqrt{3}$  times larger than the spacing in the triangular lattice formed by the projection of the columns.

(iv) A third distinct (hexagonal) crystalline phase is observed for  $\rho \approx 0.7865$  (outside the range of densities explored in Fig. 5). At this state point the liquid, after some initial equilibration, crystallizes into a crystalline phase characterized by a hexagonal symmetry of one of its crystalline planes. This crystalline type is also formed by parallel columns consisting of equidistantly spaced atoms. The spacing among these atoms is slightly larger than the hard core distance. The projection of these columns onto a perpendicular plane forms a hexagonal lattice with spacing slightly smaller than the hard core. This spacing is equal to  $\sqrt{3}/2$  of the distance between atoms in the columns. The neighboring columns are shifted with respect to each other by one-half of the atom spacing in the columns, so that the atom and its two neighbors in the neighboring column form an equilateral triangle. Thus in this crystalline type, each atom has eight nearest neighbors in its repulsive ramp, two in the same column and six in the three neighboring columns.

(v) For even larger densities not studied in this work, hexagonal close packed and finally hard-sphere face cubic centered crystals are expected [11].

We now discuss the possibility of a liquid-liquid critical point in this model. By quadratically extrapolating the isochores into the glassy state, we observe a crossing at very low temperatures. This crossing of the near density isochores is equivalent to  $\partial P/\partial V|_T=0$  and hence predicts the existence of a critical point with coordinates  $T \approx 0.025$ ,  $P \approx 0.838$ , and  $\rho \approx 0.346$ , close to the largest density at which an isochore develops a negative slope. Interestingly, the TMD line, if extrapolated, appears to go directly to this putative critical point.

Another characteristic feature is the behavior of the isothermal compressibility, which shows an anomalous increase upon cooling between the lines of maximal and minimal compressibility, is shown in Fig. 5(a). The part of the low density branch with a positive slope corresponds to a compressibility minima, while the high density branch corresponds to the compressibility maxima. As in water and other materials with density anomaly, the isothermal compressibility line crosses the TMD line at the point of its maximal temperature (vertical slope) due to the mathematical properties of the second derivative of the equation of state [37]. Again, as in water, the line of compressibility maxima, if extrapolated, seems to approach the putative critical point.

Since the RY closure is thermodynamically consistent, it is possible to evaluate the state points  $P(\rho, T)$  theoretically as well. Indeed, once the static structure factor  $S(k)$  is obtained, the pair correlation function  $g(r)$  can be calculated by taking the inverse Fourier transform of  $S(k)$ . All other thermodynamic quantities are calculated using the interparticle potential function  $U(r)$  and  $g(r)$ . In Fig. 5(c) we show the state points  $P(\rho, T)$  consisting of eight isochores of the system calculated using RY. Comparing Figs. 5(a) and 5(c), we can see that the RY predicts a smaller value of the pressure and also that the density maxima points are shifted to higher volumes. Despite this discrepancy in  $P$ , the shape of the isochores is very well reproduced. Even in the RY case, density maxima line appears in the phase diagram. While in the simulation, extremely slow dynamics prevents access to the region where the critical point is probably located, in the RY calculations, no convergence of the parameter  $\zeta$  is achieved in the same region. Again, a smooth extrapolation of the calculated isochores is consistent with a crossing point, and hence a critical point.

The thermodynamic behavior discussed above is analogous to the behavior of the one-dimensional model for which an exact solution can be obtained (see the Appendix ).

#### D. Dynamics

Next we focus on the dynamic properties of the model. Figure 5(a) shows the lines of diffusivity maxima and minima, i.e., the locus of points where  $\partial D/\partial P|_T=0$  in the phase diagram. The region of the anomalous increase of  $D$  upon compression ( $\partial D/\partial P|_T > 0$ ) embraces the region of density anomaly as it does in two-dimensional models as well as in water [4,26].

Figure 6(a) shows the density dependence of  $D$  calculated from MD along several isotherms in a density range extending to  $\rho=0.7$ . One minimum and one maximum are observed

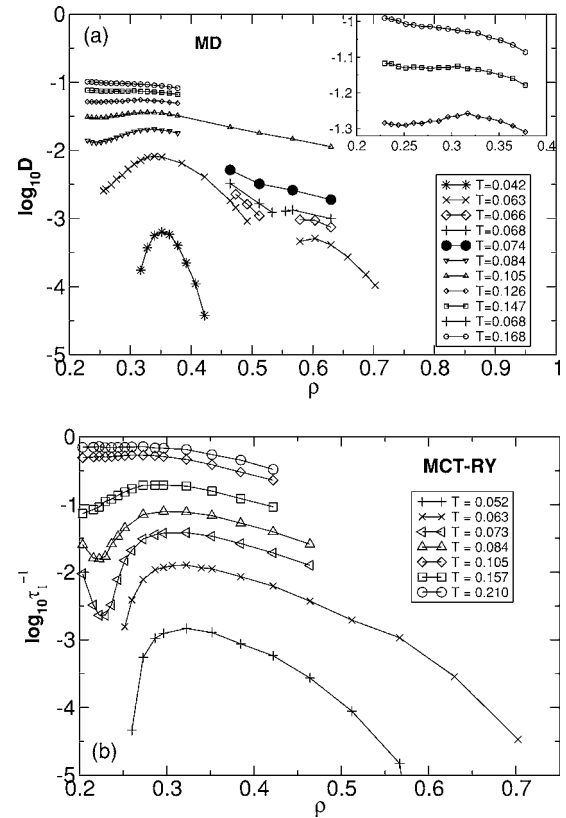


FIG. 6. (a) The behavior of the diffusion coefficient as a function of density  $\rho$  for several isotherms obtained from MD simulations. Inset shows the behavior of high temperatures. (b) The  $\alpha$ -relaxation time  $\tau_1^{-1}$  from MCT-RY. At low temperatures when the density is very high or low,  $\tau_1$  increases sharply, showing the transition to a glassy state. Note the similar behavior of  $D$  and  $\tau_1^{-1}$ .

at high  $T$  [also shown in the inset of Fig. 6(a)]. At low  $T$ , for the range of densities  $0.492 < \rho < 0.579$ , we cannot reliably measure the diffusion coefficient, because the system does not equilibrate within the simulation time. Interestingly, the system again equilibrates well for the higher densities [38].

It is interesting to compare the  $\rho$  dependence of the relaxation times calculated from MD with the prediction of mode coupling theory using RY results for  $S(q)$  (MCT-RY). A comparison with the dynamics predicted by MCT can be performed by comparing the  $T$  and  $\rho$  dependence of  $D$  with the corresponding dependence of the inverse of  $\alpha$ -relaxation time. The  $\alpha$ -relaxation time can be calculated within MCT, from the solutions of Eq. (13). More specifically, for each wave vector  $q$ , the relaxation time can be defined as the value at which  $\phi(q, t)$  reaches the value  $1/e$ . We define  $\tau_1$  and  $\tau_2$  as the relaxation times corresponding to the  $q$ -vector of the first and second peaks of the structure factor, respectively. Figure 6(b) shows the inverse of  $\alpha$ -relaxation time  $\tau_1^{-1}$  for the wave vector corresponding to the first peak of the structure factor as a function of  $\rho$  for different  $T$ . The same sequence of minima and maxima characteristic of the MD diffusivity data is found in the prediction of MCT-RY. This agreement is consistent with the possibility that the structure factor, the only input in the MCT, also encodes the system's dynamic properties.

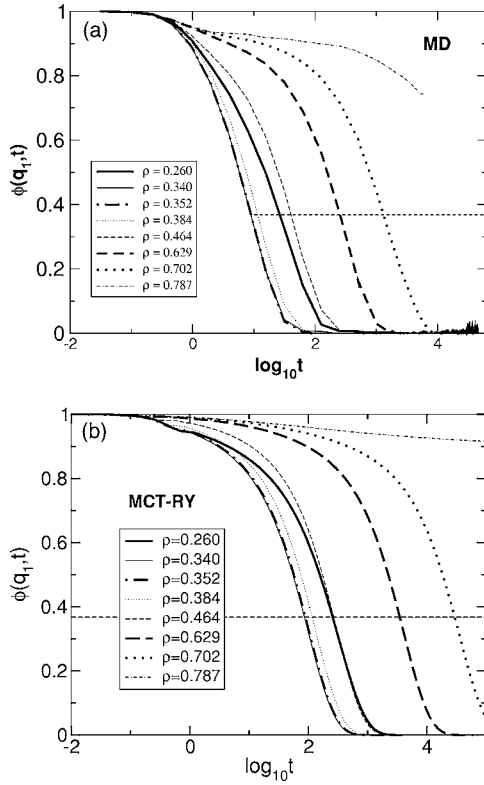


FIG. 7. The behavior of the correlators for the wave vector  $q_1$  corresponding to the first peak of the static structure factor for  $T=0.063$  for (a) MD and (b) MCT-RY. The dashed horizontal line indicates the  $1/e$  value used to define the characteristic time  $\tau_1$ .

To better characterize the low temperature dynamics and investigate the possibility of different glasses, we next study the decay of the density autocorrelation functions  $\phi(q, t)$  as a function of  $t$  at  $T=0.063$  in Fig. 7, and calculate  $\phi(q, t)$  from the MD trajectories [Fig. 7(a)]. The nonmonotonic behavior of  $D$  and  $\tau_1$  discussed in the previous figure is also seen in the decay of  $\phi(q, t)$ . At the highest studied density  $\rho > 0.787$ , the correlator does not decay to zero in the time scale of our simulations. For lower  $\rho$ , the decay becomes faster until  $\rho=0.352$  and then it starts to slow down again. For  $\rho < 0.26$ , crystallization prevents the approach to a glass state. The decay of the correlation functions (at  $q$  corresponding to the first peak of the structure factor) can be well represented via a stretched exponential decay [Eq. (15)] at very high densities,  $\rho=0.702$  ( $\beta=0.89$ ), and by simple exponential decay ( $\beta=1$ ) at low  $\rho$ . A similar behavior is seen in Fig. 7(b) where the predictions of the MCT equations are shown. Again, on decreasing  $\rho$ , first a speed-up and then a slowing down of the dynamics is observed.

To illustrate the comparison between MD and MCT-RY, we show the density dependence of  $\tau_1$  and  $\tau_2$  in Fig. 8. The two sets of data ( $\tau_1$  and  $\tau_2$  show the same anomalous behavior, with the minimum corresponding to the maximal diffusivity at the same  $\rho$ ). The minima for RY are shifted to lower densities with respect to MD at  $T=0.041$ .

It is interesting to observe that while the slowing down of dynamics can be numerically followed for a large dynamical range at a high density, a low density crystallization prevents

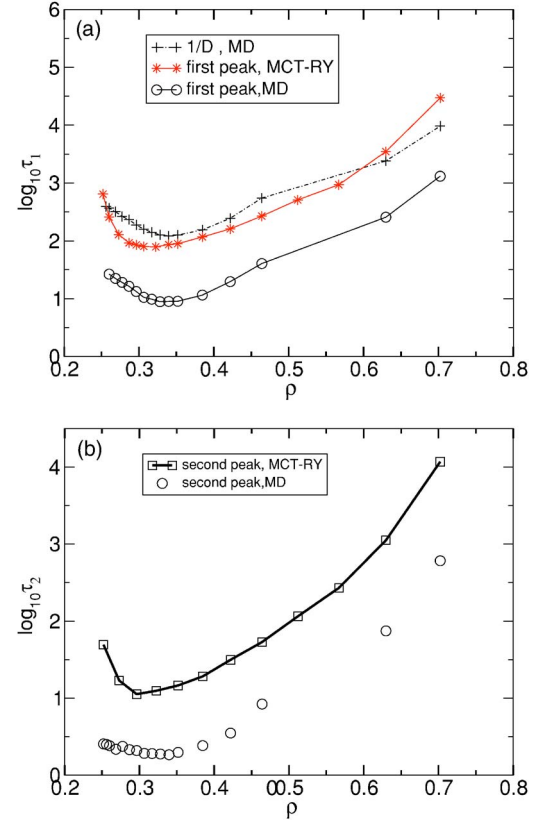


FIG. 8. (Color online) The density behavior of the relaxation times (a)  $\tau_1$ , and (b)  $\tau_2$ , obtained directly from MD simulations for  $T=0.063$  and for the MCT calculations based on RY. The behavior of the diffusion coefficient is also shown. All curves show the anomalous decrease upon compression for small densities.

the generation of a glass structure. Unlike in MD, RY solutions can be found in a wider density range. It is thus interesting to ask whether a glass line is predicted by MCT-RY at low densities and, if so, how the two glasses differ. By solving the MCT equations for a wider range of densities, we find two distinct glasses at  $T=0.052$ ,  $\rho=0.682$  and  $\rho=0.257$ . These two glasses are characterized by different critical nonergodicity parameters (shown in Fig. 9). While the low density glass nonergodicity factor is similar to the one found in hard sphere systems, the high density glass is characterized by large amplitudes both at the first and second peak of  $S(q)$ . This resembles the one found in star polymers at high density [39], though the amplitude of the second peak in the latter becomes larger than that of the first peak.

#### IV. SUMMARY AND CONCLUSIONS

In this work, we have presented a systematic numerical study of the static and dynamic properties of a system of particles interacting with a spherical repulsive potential, with a range of interaction of the order of the particle's hard-core diameter. The simplicity of the model makes it possible to study it with efficient numerical algorithms and, theoretically, with self-consistent integral theories [28]. Our results accomplish the following.

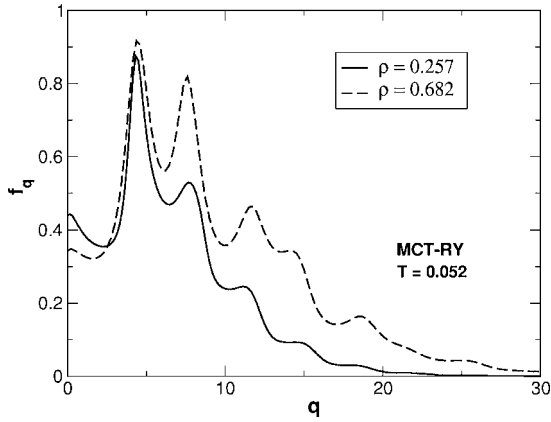


FIG. 9. The behavior for  $T=0.052$  of the critical nonergodicity parameter  $f_q$  for the two critical densities  $\rho=0.257$  and  $\rho=0.682$ .

(i) They confirm the previous theoretical calculations by Jagla [11] concerning the existence of a line of density maxima in the phase diagram of this potential. Results also provide an accurate evaluation of this line as well as of the line of compressibility maxima and minima.

(ii) They confirm that different crystal structures are found at low temperatures, depending on the density [11], and provide estimates of the homogeneous nucleation line and approximate melting lines for the liquid-crystal transitions.

(iii) They provide evidence of the possibility of a liquid-liquid critical point at  $T \approx 0.025$ ,  $P \approx 0.838$ , and  $\rho \approx 0.346$ . The location of the critical point is below the homogeneous nucleation line or the glass transition line and cannot be accessed by simulations. A theoretical RY calculation of the state points  $P(\rho, T)$  is able to reproduce the thermodynamic anomalies. These calculations also suggest the possibility of a liquid-liquid critical point but, again, its precise location cannot be determined due to the impossibility of equating the

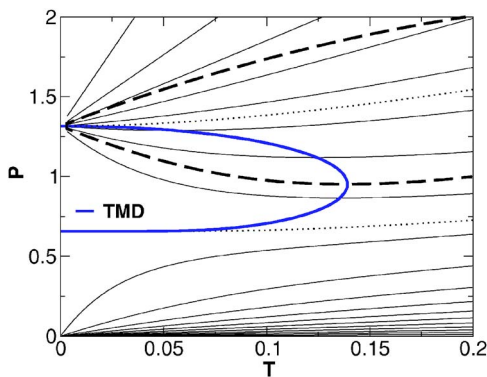


FIG. 10. (Color online) The equation of state  $P(\rho, T)$  of the one-dimensional system with the ramp potential ( $\sigma_0=1, \sigma_1=1.76, U_0=1$ ) defined in Eq. (1). The thin solid lines are isochores for  $\rho=0.05, 0.1, \dots, 0.95$  from bottom to top. The bold dotted lines are isochores for  $\rho=1/\sigma_1$  and  $\rho=\rho_c \equiv 2/(\sigma_0+\sigma_1)$  between which the density anomaly region bounded by the temperature of the maximal density line (bold blue line) is located. The dashed bold line bounds the region of anomalous increase of isothermal compressibility upon cooling indicating its extrema.

“virial” and “fluctuation” compressibilities with enough accuracy in this region of the phase diagram. Thus the existence of the critical point proposed by the extrapolation of the state points  $P(\rho, T)$  into the deeply supercooled region remains questionable [40].

(iv) They show that the RY closure agrees qualitatively with simulations of the system with the repulsive ramp potential and that it reproduces the static and dynamic anomalies. The RY closure slightly underestimates the pressure, and shifts the anomalies to a region of lower density.

(v) They provide evidence that dynamic anomalies in this model have a structural origin and they are indeed captured by the MCT-RY theory, which uses only structural information as input. Diffusion anomalies are encountered before the density anomalies, consistent with the case of water [4].

(vi) They suggest the possibility of different types of glasses in this simple system, consistent with the existence of different crystalline phases. A more extensive study based on the MCT-RY may help evaluate the location and the intersections [32,41,42] between different glass transition lines.

#### ACKNOWLEDGMENTS

The authors thank C. Likos for help with the RY closure and for extensive discussions and to L. Braunstein for help with MD calculations in the initial phases of the project. The authors also thank NSF Chemistry Grant Nos. CHE0096892 and CHE0404673 and MIUR Cofin 2001 and Fibr 2002, and MRTN-C-2003-504712 for support.

#### APPENDIX ONE-DIMENSIONAL SYSTEM

Applying the Takahashi method [43], one can find the state points  $P(\rho, T)$  for the one-dimensional system of particles interacting via the ramp potential [see Eq. (1)]. In this case, the partition function  $\Psi$  for the Gibbs potential  $G(P, T)$  can be factored, so that

$$G = -\frac{1}{\beta} N \ln \Psi(P, T), \quad (\text{A1})$$

where  $\beta = 1/k_B T$

$$\Psi(P, T) = \int_0^\infty \exp\{-\beta[U(r) + Pr]\} dr. \quad (\text{A2})$$

Substituting Eq. (1) into Eq. (A2) and integrating, we find that

$$\Psi(P, T) = \frac{\exp[-\beta(P\sigma_0 + U_0)] - \exp(-\beta P\sigma_1)}{\beta(P - P_c)} + \frac{\exp(-\beta P\sigma_1)}{\beta P}, \quad (\text{A3})$$

where  $P_c = U_0/(\sigma_1 - \sigma_0)$ . Since  $V \equiv (\partial G / \partial P)_T$ ,

$$\rho \equiv N/V = -\frac{\beta \Psi}{(\partial \Psi / \partial P)_T}, \quad (\text{A4})$$

which, after differentiation, leads to

$$\rho = \frac{\frac{e^{-\beta(U_0 + \sigma_0 P)}}{(P - P_c)} + e^{-\beta\sigma_1 P} \left( \frac{1}{P} - \frac{1}{(P - P_c)} \right)}{e^{-\beta(U_0 + \sigma_0 P)} \left( \frac{\sigma_0}{(P - P_c)} + \frac{1}{\beta(P - P_c)^2} \right) + e^{-\beta\sigma_1 P} \left( \frac{\sigma_1}{P} - \frac{\sigma_1}{(P - P_c)} + \frac{1}{\beta P^2} - \frac{1}{\beta(P - P_c)^2} \right)}. \quad (\text{A5})$$

Note that  $P_c$  plays the role of a critical pressure, at which the equation of state points  $\rho(P, T)$  becomes discontinuous for  $T \rightarrow 0$ . Indeed,

$$\lim_{T \rightarrow 0} \rho = \begin{cases} 1/\sigma_0, & P > P_c, \\ 2/(\sigma_1 + \sigma_0), & P = P_c, \\ 1/\sigma_1, & P < P_c. \end{cases} \quad (\text{A6})$$

Hence, an infinitesimal increase of pressure around  $P_c$  and small  $T$  leads to a finite increase of density from  $1/\sigma_1$  for  $P < P_c$  to  $1/\sigma_0$  for  $P > P_c$ . Thus, in the one-dimensional system, there is an analog of a critical point at  $T = T_c = 0, P = P_c$ , and  $\rho = \rho_c \equiv 2/(\sigma_1 + \sigma_0)$ , at which the isothermal compress-

ibility diverges. At  $P = P_c$ , Eq. (A5) simplifies to

$$\rho = \frac{1 + k_B T / U_0}{(\sigma_0 + \sigma_1)/2 + (k_B T / U_0) \sigma_1 + (k_B T / U_0)^2 (\sigma_1 - \sigma_0)}. \quad (\text{A7})$$

For  $P < P_c$  there exists a region in which there is a density anomaly and a region in which there is a compressibility anomaly, exactly as in the three-dimensional model studied in this work.

The isochores described by Eq. (A5) are plotted in Fig. 10. One can see that the temperature of maximal density approaches the critical point as  $P \rightarrow P_c$ .

- 
- [1] P. Debenedetti, *J. Phys.: Condens. Matter* **15**, R1669 (2003).  
[2] C. A. Angell, *Annu. Rev. Phys. Chem.* **55**, 559 (2004).  
[3] P. G. Debenedetti, *Metastable Liquids: Concepts and Principles* (Princeton University Press, Princeton, 1998).  
[4] J. R. Errington and P. G. Debenedetti, *Nature (London)* **409**, 318 (2001).  
[5] P. H. Poole, F. Sciortino, U. Essmann, and H. E. Stanley, *Nature (London)* **360**, 324 (1992); F. Sciortino, P. H. Poole, U. Essmann, and H. E. Stanley, *Phys. Rev. E* **55**, 727 (1997); S. T. Harrington, P. H. Poole, F. Sciortino, and H. E. Stanley, *J. Chem. Phys.* **107**, 7443 (1997); M. Yamada, S. Mossa, H. E. Stanley, and F. Sciortino, *Phys. Rev. Lett.* **88**, 195701 (2002).  
[6] P. H. Poole, F. Sciortino, T. Grande, H. E. Stanley, and C. A. Angell, *Phys. Rev. Lett.* **73**, 1632 (1994).  
[7] O. Mishima and H. E. Stanley, *Nature (London)* **392**, 164 (1998).  
[8] F. Sciortino, E. La Nave, and P. Tartaglia, *Phys. Rev. Lett.* **91**, 155701 (2003).  
[9] F. H. Stillinger, *Chem. Phys.* **65**, 3968 (1976).  
[10] F. H. Stillinger and D. K. Stillinger, *Physica A* **244**, 358 (1997).  
[11] E. A. Jagla, *J. Chem. Phys.* **111**, 8980 (1999); *Phys. Rev. E* **63**, 061509 (2001).  
[12] M. R. Sadr-Lahijany, A. Scala, and H. E. Stanley, *Phys. Rev. Lett.* **81**, 4895 (1998); *Phys. Rev. E* **60**, 6714 (1999).  
[13] A. Scala, M. Reza Sadr-Lahijany, N. Giovambattista, S. V. Buldyrev, and H. E. Stanley, *J. Stat. Phys.* **100**, 97 (2000); *Phys. Rev. E* **63**, 041202 (2001).  
[14] S. V. Buldyrev, G. Franzese, N. Giovambattista, G. Malescio, M. Reza Sadr-Lahijany, A. Scala, A. Skibinsky, and H. E. Stanley, in *New Kinds of Phase Transitions: Transformations in Disordered Substances*, NATO Advanced Research Workshop, Volga River, edited by S. V. Brazhkin, S. V. Buldyrev, V. Ryzhov, and H. E. Stanley, (Kluwer, Dordrecht, 2002), pp. 97–120.  
[15] P. C. Hemmer and G. Stell, *Phys. Rev. Lett.* **24**, 1284 (1970); G. Stell and P. C. Hemmer, *J. Chem. Phys.* **56**, 4274 (1972); J. M. Kincaid and G. Stell, *ibid.* **67**, 420 (1977); J. M. Kincaid, G. Stell, and E. Goldmark, *ibid.* **65**, 2172 (1976); J. M. Kincaid, G. Stell, and C. K. Hall, *ibid.* **65**, 2161 (1976).  
[16] G. Franzese, G. Malescio, A. Skibinsky, S. V. Buldyrev, and H. E. Stanley, *Nature (London)* **409**, 692 (2001).  
[17] V. N. Ryzhov and S. M. Stishov, *Phys. Rev. E* **67**, 010201 (R) (2003).  
[18] A. Lang, G. Kahl, C. N. Likos, H. Lowen, and M. Watzlawek, *J. Phys.: Condens. Matter* **11**, 10143 (1999).  
[19] C. N. Likos, H. Lowen, M. Watzlawek, B. Abbas, O. Jucknischke, J. Allgaier, D. Richter, *Phys. Rev. Lett.* **80**, 4450 (1998).  
[20] M. Watzlawek, C. N. Likos, and H. Löwen, *Phys. Rev. Lett.* **82**, 5289 (1999).  
[21] M. Laurati, J. Stellbrink, R. Lund, L. Willner, D. Richter, and E. Zaccarelli, *Phys. Rev. Lett.* **94**, 195504 (2005).  
[22] U. Bengtzelius, W. Götze, and A. Sjöander, *J. Phys. C* **17**, 5915 (1984).  
[23] W. Götze, in *Liquids, Freezing, and Glass Transition*, edited by J. P. Hansen, D. Levesque, and J. Zinn-Justin (North-Holland, Amsterdam, 1991), p. 287.  
[24] D. C. Rapaport, *The Art of Molecular Dynamic Simulation* (Cambridge University Press, Cambridge, 1995).  
[25] A. Skibinsky, S. V. Buldyrev, G. Franzese, G. Malescio, and H. E. Stanley, *Phys. Rev. E* **69**, 061206 (2004).  
[26] S. V. Buldyrev, G. Franzese, N. Giovambattista, G. Malescio, M. R. Sadr-Lahijany, A. Scala, A. Skibinsky, H. E. Stanley, *Physica A* **304**, 23 (2002).  
[27] J. P. Hansen and I. R. McDonald, *Theory of Simple Liquids* (Academic, London, 1976).

[28] C. Caccamo, Phys. Rep. **274**, 1 (1996).  
 [29] F. J. Rogers and D. A. Young, Phys. Rev. A **30**, 999 (1984).  
 [30] C. Mayer, C. N. Likos, and H. Löwen, Phys. Rev. E **70**, 041402 (2004).  
 [31] For the case of slow dynamics in water see, for example, F. Sciortino, P. Gallo, P. Tartaglia, and S. H. Chen, Phys. Rev. E **54**, 6331 (1996); F. Sciortino, L. Fabbian, S. H. Chen, and P. Tartaglia, *ibid.* **56**, 5397 (1997); L. Fabbian, F. Sciortino, and P. Tartaglia, J. Non-Cryst. Solids **235–237**, 350 (1998); F. Starr, F. Sciortino, and H. E. Stanley, Phys. Rev. E **60** 6757 (1999).  
 [32] E. Zaccarelli, G. Foffi, K. A. Dawson, S. V. Buldyrev, F. Sciortino, and P. Tartaglia, Phys. Rev. E **66**, 041402 (2002).  
 [33] For a recent review on the comparison between experimental data and MCT predictions see W. Götze, J. Phys.: Condens. Matter **11**, A1 (1999).  
 [34] M. Nauroth and W. Kob, Phys. Rev. E **55**, 675 (1997); C. Theis *et al.*, *ibid.* **62**, 1856 (2000); F. Sciortino and W. Kob, Phys. Rev. Lett. **86**, 648 (2001).  
 [35] M. Watzlawek, C. N. Likos, and H. Loewen, J. Phys.: Condens. Matter **10**, 8189 (1998).  
 [36] <http://www.ccl.net/chemistry/resources/software/X-WINDOW/xbs/index.shtml>  
 [37] S. Sastry P. G. Debenedetti, F. Sciortino, and H. E. Stanley, Phys. Rev. E **53** 6144 (1996).  
 [38] One may expect that this part of the phase diagram corresponds to partial crystallization. However, the behavior of the system in this region of the phase diagram does not resemble crystallization, which at other regions of the phase diagram is characterized by a sharp decrease of potential energy with a latent heat release. The potential energy at these state points slowly decreases with time, resembling the aging of glasses. Also, upon heating to a slightly larger temperature,  $T = 0.0684$  (for which no anomalous behavior of diffusion coefficient is observed), the system slowly relaxes back to the normal liquid phase. In contrast, spontaneous crystallization usually happens in a deeply supercooled state so that the true crystal does not melt if the temperature is slightly increased. Also, the structure factors of these phases do not develop large, high  $q$  peaks, characteristic of the crystalline phase. Thus the nature of these intermediate phases is not clear.  
 [39] G. Foffi, F. Sciortino, P. Tartaglia, E. Zaccarelli, F. Lo Verso, L. Reatto, K. A. Dawson, and C. N. Likos, Phys. Rev. Lett. **90**, 238301 (2003).  
 [40] E. A. Jagla, Braz. J. Phys. **34**, 17 (2004).  
 [41] L. Fabbian *et al.*, Phys. Rev. E **59**, R1347 (1999); **60**, 2430(E) (1999); F. Sciortino, Nat. Mater. **1**, 45 (2002).  
 [42] K. Dawson, G. Foffi, M. Fuchs, W. Gotze, F. Sciortino, M. Speri, P. Tartaglia, Th. Voigtmann, and E. Zaccarelli, Phys. Rev. E **63**, 011401 (2000).  
 [43] E. H. Lieb and D. C. Mattis, *Mathematical Physics in One Dimension* (Academic, New York, 1966), p. 2.